Contrasting Cloud Radiative Feedbacks during Warm Pool and Cold Tongue El Niños

Lin Chen[1, 2, 3], Lu Wang[1, 2, 3], Tim Li[1, 3], and De-Zheng Sun[4]

[1] *Key Laboratory of Meteorological Disaster, Ministry of Education (KLME) / Joint International Research Laboratory of Climate and Environmental Change (ILCEC) / Collaborative Innovation Center on Forecast and Evaluation of Meteorological Disasters (CIC-FEMD), Nanjing University of Information Science and Technology, Nanjing, China*
[2] *Laboratory for Regional Oceanography and Numerical Modeling, Qingdao National Laboratory for Marine Science and Technology, Qingdao, China*
[3] *International Pacific Research Center, and School of Ocean and Earth Science and Technology, University of Hawai'i at Mānoa, Honolulu, Hawaii, USA*
[4] *Department of Atmospheric and Oceanic Sciences, University of Colorado, Boulder, Colorado, USA*

Abstract

The study presents the contrasting characteristics of cloud-radiative feedbacks to the cold tongue (CT) and warm pool (WP) El Niño (EN). The maximum sea surface temperature anomalies (SSTA) of the CT-EN are located in the far-eastern Pacific. However, the maximum responses of the shortwave- and longwave-cloud-radiative forcing (SWCRF and LWCRF) to the CT-EN warming are centered near the dateline, showing 70° westward shift relative to the maximum SSTA center of CT-WN. In contrast, the maximum responses of the SWCRF and LWCRF to the WP-EN warming show only slight westward shift relative to the maximum SSTA center. The contrasting cloud-radiative feedbacks to the two types of ENs can be traced back to the contrasting precipitation feedbacks, which is associated with the convection threshold. When the warm SSTA of CT-EN occurs in the relatively cold eastern Pacific, the total SST in-situ may not exceed the convection threshold. Therefore, the induced precipitation anomaly would occur towards the warm western Pacific, and the corresponding cloud cover and cloud-radiative feedbacks would exhibit an apparent westward shift. As the warm SSTA of WP-EN occurs in the relatively warm central Pacific, the corresponding responses of the anomalous fields to the WP-EN show only slight westward displacement.

(**Citation**: Chen, L., L. Wang, T. Li, and D.-Z. Sun, 2018: Contrasting cloud radiative feedbacks during warm pool and cold tongue El Niños. *SOLA*, **14**, 126−131, doi:10.2151/sola.2018-022.)

1. Introduction

Cloud is the prominent modulator in the climate system (Hartmann and Short 1980; Kiehl and Trenberth 1997; Houghton et al. 2001). Through the radiative effects, the cloud could regulate the global energy distribution and thereby alter the atmospheric circulation, which in turn modulates their effects (Stephens 2005). Thus it is critical to understand the cloud-radiative feedback in the climate system (Cess et al. 1989; Ramanthan et al. 1989; Sun and Held 1996).

A number of previous studies have devoted great efforts into investigating the cloud-radiative feedbacks in climate system (Ramanthan et al. 1989; Cess et al. 1990; Sun and Held 1996; Soden 1997; Schneider et al. 1999; Soden and Held 2006; Sun et al. 2003, 2006, 2009; Zhu et al. 2007; Zhang and Sun 2008; Wu et al. 2011; Zheng et al. 2014; Li et al. 2014, 2015). As El Niño-Southern Oscillation (ENSO) is the greatest natural climate

variability on interannual timescale and exerts profound impacts on the global climate and weather (Philander 1990; Wang and Chen 2016, 2017a, b; Yang et al. 2018), a frequently used method to quantify the cloud-radiative feedbacks is to calculate the response of cloud-radiative forcing to the sea surface temperature (SST) changes on the time scale of ENSO (Sun and Held 1996; Soden 1997; Sun et al. 2003, 2006, 2009; Chen et al. 2013, 2015, 2017; Hu et al. 2017). For example, through calculating the response of cloud-radiative forcing to El Niño (hereinafter EN) warming, some previous studies evaluated the cloud-radiative feedbacks in the ENSO cycle in coupled model simulations (e.g., Sun and Held 1996; Soden 1997; Sun et al. 2006; Sun et al. 2009; Chen et al. 2013, 2016a).

More recently, plenty of studies pointed out that there is a new type of EN which tends to occur more frequently since the late 1990s (Chung and Li 2013; Xiang et al. 2013; Zhou et al. 2014). In contrast to the canonical EN featured by the prominent warming in the eastern equatorial Pacific and the coast of South America, the warming center of the new type EN occurs in the central Pacific (e.g., Ashok et al. 2007; Kao and Yu 2009; Kug et al. 2009). Such a new type of EN has various terminologies, such as dateline El Niño, El Niño Modoki, CP El Niño, and warm pool El Niño. In the following discussion, we use the warm pool El Niño (hereinafter WP-EN) to term the new type of EN and the cold tongue El Niño (hereinafter CT-EN) to term the canonical EN. The distinctive EN warming patterns may induce different teleconnections (e.g., Ashok et al. 2007; Weng et al. 2007; Feng et al. 2016a, 2016b, 2017; Xu et al. 2017a, 2017b, 2018). For instance, Hu et al. (2016) pointed out contrasting contributions from the thermodynamic and dynamical processes to the SSTA associated with the two types of ENs, through performing a feedback attribution analysis. Hence, it is conceivable that the responses of cloud-radiative forcing to the two types of EN may differ from each other. However, it is not clear about the specific characteristics of the response of cloud-radiative effects to the new type of EN and whether it is different from that to conventional CT-EN.

To shed some light on the characteristics of cloud-radiative feedbacks to the new type of EN, we may use the aforementioned method that was previously employed to detect the cloud-radiative feedbacks in ENSO cycle. With the advent of satellite data, it is possible to quantify the cloud radiation forcing effects at the top of atmosphere (TOA) more accurately than the results derived from the surface heat flux reanalysis. Through classifying the ENSO into two specific types, the current study aims to identify the primary characteristics of the cloud-radiative feedbacks to the two types of EN.

The rest of this paper is organized as follows. The datasets and methods are described in Section 2. The contrasting characteristics of the cloud-radiative feedbacks to the two types of EN are presented in Section 3. The possible explanation of the contrasting
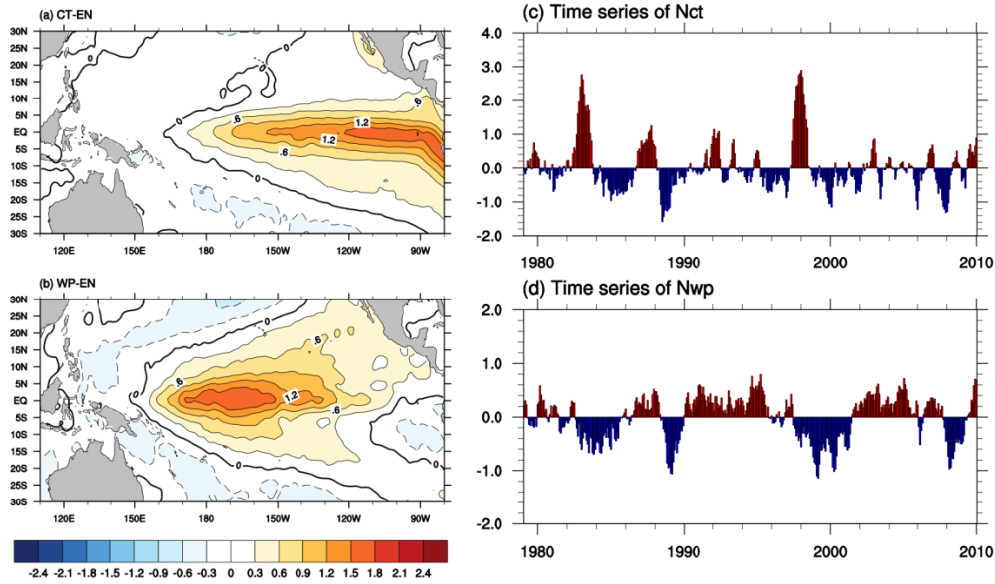

Fig. 1. The horizontal patterns of SSTA pattern regressed onto (a) the cold tongue EL Niño (CT-EN) index and (b) the warm pool El Niño (WP-EN) index (unit: K/K). Time series of (c) the CT-EN index and (d) WP-EN index (unit: K), which are derived from the HadISST data for 1979−2009. For detailed description about the CT-EN and WP-EN indexes, refer to the body text.

cloud-radiative feedbacks is provided in Section 4. Finally, a summary is shown in Section 5.

2. Data and methods

The monthly SST used in this study is from the HadISST dataset (Rayner et al. 2003) during 1979−2009. The monthly datasets of the radiative fluxes and cloud cover are from the International Satellite Cloud Climatology Project (ISCCP; Zhang et al. 2004) covering 1984−2009. The monthly precipitation data is from the Global Precipitation Climatology Project (GPCP; Huffman et al. 2009) during 1979−2009. The monthly data for the vertical velocity at 500 hPa during 1979−2009 is provided by the ECMWF reanalysis product (ERA-interim; Dee et al. 2011). In this study, the anomalies indicate the interannual anomaly fields which were obtained through removing their corresponding climatological seasonal cycle.

To estimate the responses of cloud-radiative forcing to the two types of EN regimes, we will apply the method used in previous studies (e.g., Sun et al. 2003, 2006, 2009; Chen et al. 2013): quantifying the feedbacks through regressing the corresponding anomaly fields to the SSTA. In these previous studies, the SSTA averaged over a wide region (5°S−5°N, 150°E−110°W) was used to do the regression analysis. To identify the contrasting characteristics of the cloud-radiative feedbacks to the two types of EN, in this study the corresponding anomaly fields are, respectively, regressed to the CT-EN index and WP-EN index. Based on the definition proposed by previous study (see the equation 1 in Ren and Jin 2011), we obtained the CT-EN index and WP-EN index. Figures 1a and 1b show the spatial warming patterns of CT-EN and WP-EN, which are obtained through regressing the SSTA onto the CT-EN index and WP-EN index. Clearly, the CT-EN and WP-EN shows different spatial pattern in terms of locations of SSTA warming: the maximum center of SSTA warming of the former is located near 100°W, and the latter near 170°W. Such CT- and WP- warming patterns resemble that revealed by some other studies (e.g., Ashok et al. 2007; Kao and Yu 2009; Kug et al. 2009). The specific time series of CT-EN index and WP-EN index are shown in Figs. 1c and 1d. The correlation between the Niño3 index and CT-EN index is 0.98, and the correlation between the WP-EN index and the El Niño Modoki index (EMI, which is proposed by Ashok et al. 2007) is 0.75. Note that the primary

characteristics of the feedbacks to the two types of EN are not sensitive to the selection method that is used to classify the two types of EN. The Niño3 index and EMI index have also been used to calculate the corresponding results of the feedbacks to the two types of EN (figure not shown), which resemble that shown as below.

3. Contrasting characteristics of cloud-radiative feedbacks to the two types of EN warming

The shortwave cloud radiative forcing (SWCRF) at TOA is defined as below:

$$SWCRF = SW − SW_c \qquad (1)$$

where SW and SW_c represent the TOA net downward solar radiation for the average cloudy conditions and clear sky, respectively. Following previous studies (Chen et al. 2013; Li et al. 2014, 2015), we obtained the SWCRF feedbacks to the two types of EN warming through regressing the anomalous SWCRF onto the CT-EN index and WP-EN index, respectively.

Figure 2 presents the basin-wide view of the response of SWCRF (hereafter SWCRF feedback) to the two types of ENs. Pronounced negative SWCRF anomalies are noted over the central and eastern equatorial Pacific, in response to the CT-EN warming (Fig. 2a). The SWCRF feedback to the CT-EN is characterized by an anomalous negative center of SWCRF to the east of the dateline (around 170°W), while the negative SWCRF feedback in the far-eastern Pacific is minor. Notably, the maximum center of SWCRF response exhibits a 70° longitude shift compared to the corresponding maximum SSTA center (located near 100°W, as shown in Fig. 1a). As shown in Fig. 2b, significantly negative SWCRF anomalies are found in the central equatorial Pacific, in response to the WP-EN warming. Furthermore, the maximum center SWCRF response to the WP-EN is located to the west of the dateline (around 170°E), showing only 20° displacement compared to the corresponding maximum SSTA center of WP-EN. Additionally, the maximum center of SWCRF response to CT-EN and WP-EN are, respectively, around −20 W m^{-2} K^{-1} and −36 W m^{-2} K^{-1}. This indicates a weaker SWCRF feedback over the central equatorial Pacific to CT-EN than that to WP-EN.

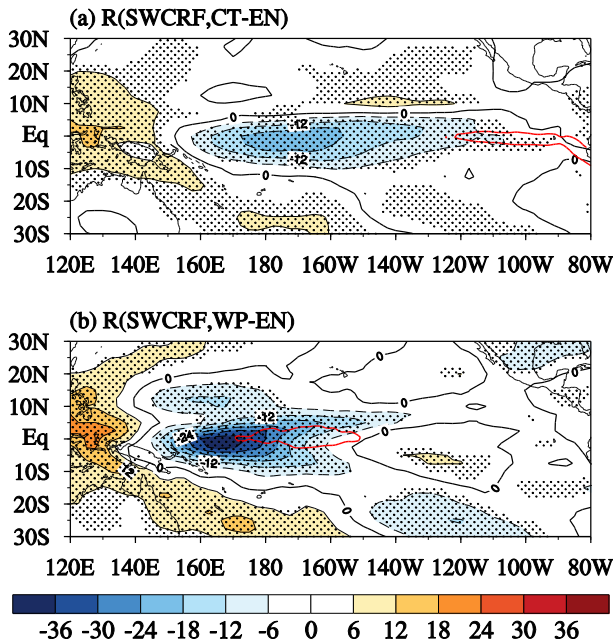The longwave cloud radiative forcing (LWCRF) is defined as below:

Fig. 2. (a) The horizontal pattern of the response of shortwave cloud radiative forcing (SWCRF) to the cold tongue El Niño warming (unit: W m^{-2} K^{-1}), which is obtained through regressing the monthly-mean SWCRF anomaly field onto the CT-EN index for the period of 1984−2009. The red line indicates the maximum center of CT-EN warming, as presented in Fig. 1a. (b) same as (a), but for the response of anomalous SWCRF to the warm pool El Niño warming that was obtained through regressing the SWCRF anomaly onto the WP-EN index. The stippling indicates the regression coefficient exceeding a confidence level of 99% using Student's t test.

Fig. 3. Same as Fig. 2, but for the response of longwave cloud radiative forcing (LWCRF) (unit: W m^{-2} K^{-1}).

$$LWCRF = F_c - F \qquad (2)$$

where F and F_c indicate the outgoing longwave radiation for the average cloudy condition and clear sky, respectively. Figure 3 provides the horizontal pattern of the response of LWCRF (hereafter LWCRF feedback) to the CT-EN and WP-EN. It is noted that positive LWCRF anomalies appear over the central and eastern equatorial Pacific (Fig. 3a), in response to the CT-EN warming. This LWCRF feedback to the CT-EN is characterized by an anomalous positive center of LWCRF to the east of the dateline (around 170°W), showing a 70° longitude shift compared to the corresponding maximum SSTA center (100°W) of CT-EN. In contrast, the maximum center of the response of LWCRF to WP-EN is located near 170°E (Fig. 3b), which shows slightly westward shift (around 20° longitude) relative to the maximum SSTA center of WP-EN. Additionally, the maximum center of the response of the LWCRF to the CT-EN and WP-EN are, respectively, 16 W m^{-2} K^{-1} and 30 W m^{-2} K^{-1}, showing a weaker LWCRF feedback over the central equatorial Pacific to CT-EN than that to WP-EN.

The different displacement configuration and the contrasting magnitude of the cloud-radiative feedbacks between the two types of ENs, may have an impact on the EN development and the ultimate EN intensity (Xiang et al. 2012; Su et al. 2014; Chen et al. 2016b, c; Chen and Li 2017). Previous studies suggested that the SWCRF feedback, a dominant thermodynamic damping feedback during ENSO cycle, plays an essential role in suppressing the ENSO development (e.g., Li et al. 2014, 2015). As demonstrated above, the SWCRF feedback to the two types of ENs show different extent of westward displacement relative to the corresponding maximum SSTA center. For the WP-EN, as the majority of the anomalous negative SWCRF is located in the central equatorial Pacific, it acts to directly damp the development of WP-EN SSTA signals in the central equatorial Pacific. But for the CT-EN, as the anomalous negative SWCRF occurs in the central equatorial Pacific and the majority of SSTA signals occur in the eastern Pacific,
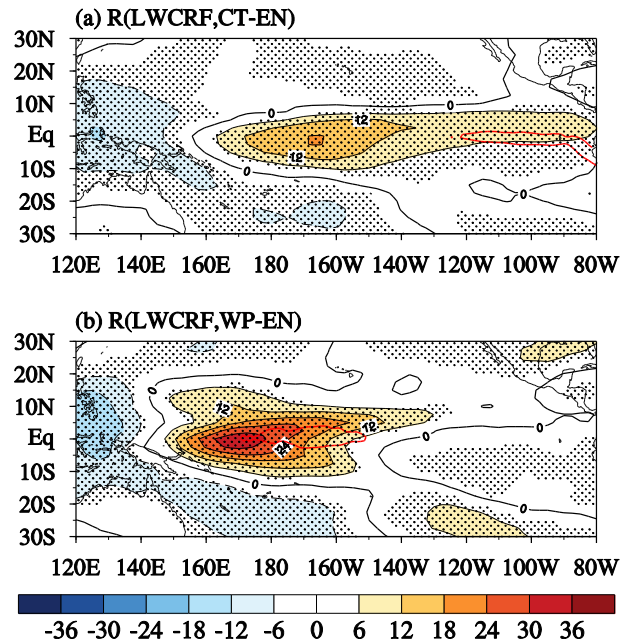
the anomalous negative SWCRF would not damp the development of CT-EN SSTA as effectively as that for the WP-EN. Moreover, the negative SWCRF feedback itself is weaker for the CT-EN than that for the WP-EN. This may play a partial role in leading to the difference in the EN intensity between the CT-EN and WP-EN (in observations, the CT-EN is usually stronger than the WP-EN, as analyzed by Zheng et al. 2014; Fang et al. 2015).

4. Possible explanation of the contrasting cloud-radiative feedbacks

To understand the contrasting characteristics of the cloud-radiative feedbacks to two types of ENs, we first examined the total cloud cover (TCC) feedback. As shown in Fig. 4, the spatial patterns of the response of TCC anomaly to the two types of EN warming mirror those of both the SWCRF and the LWCRF feedback patterns. Specifically, the maximum center of TCC feedback to CT-EN is located to the east of the dateline (near 170°W), showing about 70° westward shift relative to the maximum SSTA center of CT-EN. In contrast, the maximum center of TCC feedback to WP-EN is located near 170°E, showing a slightly westward shift (around 20° longitude) relative to the maximum SSTA center of WP-EN. Also, the maximum center of the TCC feedback to the CT-EN is weaker than that to the WP-EN. As the cloud could increase the planet albedo compared to cloudless sky, the contrasting TCC feedbacks to the two types of EN generally determine the different distribution and strength of the SWCRF feedbacks to the two types of EN. As the cloud could decrease the outgoing longwave radiation (i.e., heat preserving effect), the contrasting TCC feedbacks also cause the contrasting pattern and strength of the LWCRF feedbacks.

It is well known that the TCC feedback is closely linked to the precipitation feedback during ENSO cycle (e.g., Sun et al. 2009; Li et al. 2014). As shown in Fig. 5, the horizontal pattern of the response of precipitation (hereafter precipitation feedback) to CT-EN resembles the corresponding TCC feedback to CT-EN. So does the precipitation feedback to WP-EN. This indicates that the contrasting characteristic of the cloud-radiative and TCC feedbacks can be traced back to the different precipitation feedbacks. We further examined the response of the atmospheric circulation to the two types of EN. Figure 6 shows the spatial pattern of
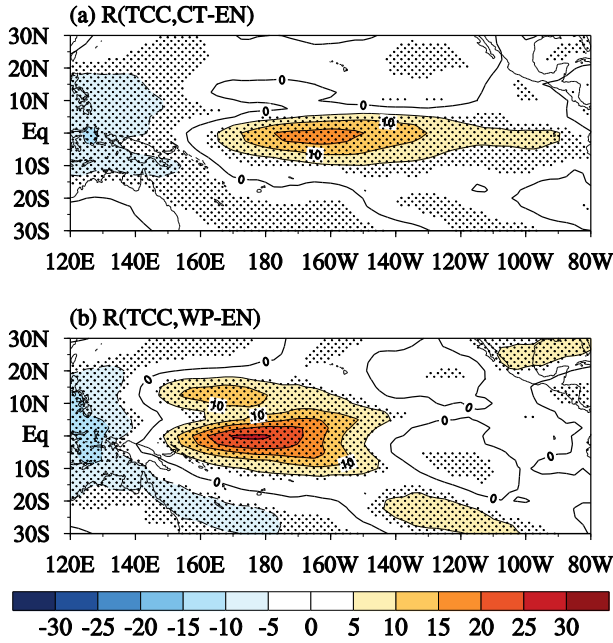
(a) R(TCC,CT-EN)

(b) R(TCC,WP-EN)

-30 -25 -20 -15 -10 -5 0 5 10 15 20 25 30

Fig. 4. As in Fig. 2, but for the response of total cloud cover (TCC) (unit: % K^{-1}).

(a) R(Precip,CT-EN)

(b) R(Precip,WP-EN)

-5 -4 -3 -2 -1 0 1 2 3 4 5

Fig. 5. The shading and the stippling are same as in Fig. 2, but for the response of precipitation (unit: mm day^{-1} K^{-1}). The contours indicate the corresponding total SST (the values are 28, 29, and 30°C) during CT-EN (Fig. 5a) and WP-EN (Fig. 5b). Here the total SST in Fig. 5a was estimated based on the following formula: $SST\_total_{CT} = \overline{SST} + SSTA_{CT} * Scale\_coeff_{CT}$, where SST_total_{CT} denotes the estimated total SST during CT-EN, $\overline{SST}$ denotes the climatological mean SST, $SSTA_{CT}$ denotes the spatial pattern of SSTA as shown in Fig. 1a, and the $Scale\_coeff_{CT}$ denotes the scale up coefficient, i.e., the average of the specific CT-EN index that exceeds 1.5 standard deviation of CT-EN index as shown in Fig. 1c. Similarly, the estimated SST_total_{WP} was obtained.

(a) R(w500hPa,CT-EN)
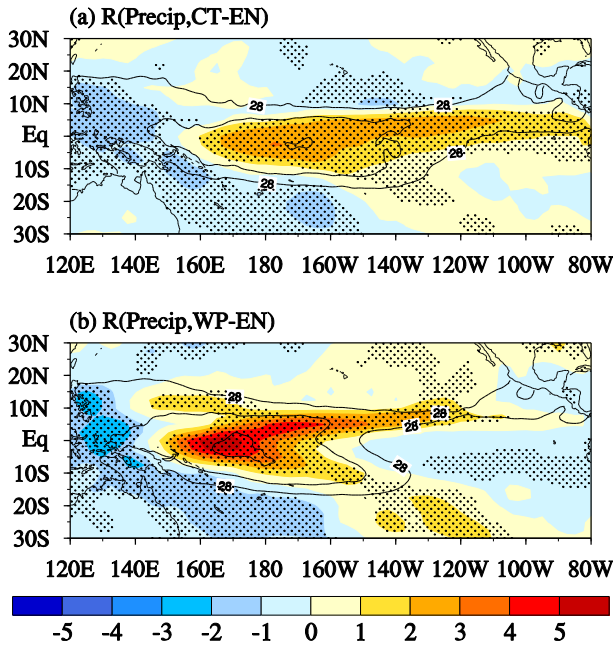
(b) R(w500hPa,WP-EN)

-60 -50 -40 -30 -20 -10 0 10 20 30 40 50 60

Fig. 6. As in Fig. 2, but for the response of vertical velocity at 500 hPa (unit: hPa day^{-1} K^{-1}).

ascending motion occurs in the central-eastern equatorial Pacific with a maximum center near 170°W (Fig. 6a), which exhibits an apparent westward shift relative to the maximum SSTA center of CT-EN. For the response to the WP-EN, the maximum center of the anomalous ascending motion is located near 170°E (Fig. 6b), which exhibits a slightly westward shift relative to its maximum SST center. Thus, the contrasting responses of atmospheric circulation to the two types of ENs match well with the contrasting precipitation feedbacks.

Regarding the contrasting characteristics of the precipitation feedbacks to the two types of EN, this may be closely associated with the tropical convection threshold. As presented in Figs. 5a and 5b, the contours indicate the total SST during the CT-EN warming and WP-EN warming. Clearly, the response of precipitation anomaly to either CT-EN or WP-EN generally occurs within the area where the total SST exceeds 28°C (Fig. 5), rather than the area where the SSTA dominates as shown in Figs. 1a and 1b. Additionally, both the maximum convection centers in response to the two types of ENs roughly coincide with the area exceeding 30°C. The well matching between the 28 isotherm and the anomalous precipitation response pattern indicates that the contrasting characteristics of the precipitation feedbacks, and the resultant TCC feedbacks and the cloud-radiative feedbacks may root in the deep convection threshold. As we know, the deep convection generally occurs when the total SST exceeds 28°C. Since the warming SSTA of the CT-EN occurs in the eastern equatorial Pacific, overlaying relatively cold climatological SST, the total SST (i.e., SSTA plus mean SST) in the eastern Pacific may not exceed the convection threshold. Thus, the occurrence of the convection would ultimately shift toward the western equatorial Pacific region, where the mean SST is warmer than that in far-eastern Pacific. Consistent with the response of precipitation to the CT-EN, the corresponding responses of the atmospheric circulation, cloud cover and cloud-radiative effects also exhibit an evident westward shift relative to the maximum center of SSTA. In contrast, the SSTA warming of WP-EN occurs in the central equatorial Pacific, overlaying relatively warm climatological SST, hence, the corresponding responses of the anomalous fields exhibit only a slightly westward shift relative to the WP-EN warming.

The difference in the magnitudes of the cloud-radiative feedback is associated with the contrasting displacement configuration between the two types of ENs. For the WP-EN, the precipitation

the response of vertical motion at 500 hPa to the two types of EN warming. As shown in Fig. 6, the vertical motion anomalies show spatial patterns that are dynamically coherent with the precipitation feedbacks. In response to the CT-EN, anomalous

response to WP-EN warming exhibits only slight displacement relative to the corresponding maximum SSTA. In contrast, for the CT-EN, the maximum precipitation response occurs near the date-line (around 170°E−150°W on the equator), but the warm SSTA signals are relatively weak near the dateline, as the region is outside the core region of CT-EN warming. Thus, the magnitudes of the precipitation feedback and the corresponding cloud-radiative feedbacks to CT-EN warming are weaker than the counterparts to WP-EN warming.

5. Summary and discussion

The study presents the contrasting characteristics of cloud-radiative feedbacks to the cold tongue and warm pool ENs. The warm SSTA of the conventional CT-EN is confined to the far-eastern Pacific, but the maximum center of the cloud-radiative feedbacks (both SWCRF and LWCRF feedbacks) to the CT-EN is located near the dateline, showing about 70° westward shift relative to its maximum SSTA center. In contrast, the maximum center of the cloud-radiative feedbacks to the WP-EN warming shows only a slightly westward displacement. Additionally, the magnitude of the SWCRF and LWCRF feedbacks to the CT-EN are weaker than that to WP-EN.

The contrasting characteristics (e.g., location and strength) of the cloud-radiative feedbacks to the two types of EN are linked to the contrasting TCC and precipitation feedbacks. Matching well with the contrasting cloud-radiative feedbacks, the TCC feedbacks also exhibit the contrasting characteristics between the two types of ENs. The different extent of the westward displacement of the TCC feedbacks relative to the corresponding maximum SSTA center are responsible for the contrasting cloud-radiative feedbacks, as the cloud is the primary contributor to the planetary albedo and has the heat preserving effect through reducing the outgoing longwave radiation. Furthermore, the contrasting TCC feedbacks can be traced back to the contrasting precipitation feedbacks. The maximum response centers of the precipitation to the two types of ENs exhibit different extent of westward displacement relative to the corresponding maximum SSTA centers. Such contrasting precipitation feedbacks are responsible for the contrasting characteristics of the cloud cover and the cloud-radiative feedbacks between the two types of ENs.

The different extent of the westward displacement of the precipitation feedbacks relative to the corresponding maximum SSTA center are associated with the tropical deep convection. The spatial patterns of the anomalous precipitation response to the two types of ENs generally match well with the 28 isotherm. When the warming SSTA of the CT-EN occurs in the eastern equatorial Pacific where the climatological SST is cold, the total SST in eastern Pacific may not exceed the convection threshold. The occurrence of the convection would ultimately shift toward the western equatorial Pacific where the climatological SST is warmer than eastern Pacific. Therefore, the response of precipitation and the corresponding responses of the large-scale atmosphere circulation, cloud cover and cloud-radiative effects show an evident westward shift relative to the maximum center of SSTA, and exhibit relatively weak intensity. In contrast, when the SSTA warming of WP-EN occurs in the central equatorial Pacific where climatological SST is relatively warm, the corresponding responses of the anomaly fields show only slightly westward shift relative to the WP-EN warming, and exhibit a relatively strong intensity.

Understanding the different ENSO responses to the two types of ENs are of importance, as the contrasting characteristics of the cloud-radiative feedbacks could make a contribution to the contrasting properties between CT-EN and WP-EN. For example, the different displacement configuration and the contrasting magnitude of the negative SWCRF feedback may play a partial role in causing the relatively strong CT-EN but relatively weak WP-EN, as also discussed by Zheng et al. (2014) and Fang et al. (2015). Hu et al. (2016) suggested that the strong water-vapor feedback over the eastern Pacific and the strong negative feedbacks over the central equatorial Pacific can help relocate the maximum warming center from the central Pacific to the eastern basin for the CT-EN. The present finding of the spatial shift of the negative SWCRF feedback in response to the CT-EN suggests that the understanding about the role of SWCRF feedback in the life cycle of El Niño only applies well to the WP-EN. It appears that the SWCRF feedback amplifies the canonical CT-EN in a relative sense because it damps the west side of CT-EN warming while it has relatively little effect on the far east side of the warming.

Reference

Ashok, K., S. K. Behera, S. A. Rao, H. Weng, and T. Yamagata, 2007: El Niño Modoki and its possible teleconnection. *J. Geophys. Res.*, **112**.

Cess, R. D., and co-authors, 1989: Interpretation of cloud-climate feedback as produced by 14 atmospheric general circulation models. *Science*, **245**, 513−516.

Cess, R. D., and co-authors, 1990: Intercomparison and interpretation of climate feedback processes in 19 atmospheric general circulation models. *J. Geophys. Res. Atmos.*, **95**, 16601−16615.

Chen, L., Y. Yu, and D.-Z. Sun, 2013: Cloud and water vapor feedbacks to the El Niño warming: Are they still biased in CMIP5 models? *J. Climate*, **26**, 4947−4961.

Chen, L., T. Li, and Y. Yu, 2015: Causes of strengthening and weakening of ENSO amplitude under global warming in four CMIP5 models. *J. Climate*, **28**, 3250−3274, doi: 10.1175/jcli-d-14-00439.1.

Chen, L., Y. Yu, and W. Zheng, 2016a: Improved ENSO simulation from climate system model FGOALS-g1.0 to FGOALS-g2. *Climate Dyn.*, **47**, 2617−2634, doi:10.1007/s00382-016-2988-8.

Chen, M., T. Li, X. Shen, and B. Wu, 2016b: Relative roles of dynamic and thermodynamic processes in causing evolution asymmetry between El Niño and La Niña. *J. Climate*, **29**, 2201−2220, doi:10.1175/JCLI-D-15-0547.1.

Chen, L., T. Li, S. K. Behera, and T. Doi, 2016c: Distinctive precursory air-sea signals between regular and super El Niños. *Adv. Atmos. Sci.*, **33**, 996−1004, doi:10.1007/s00376-016-5250-8.

Chen, L., T. Li, Y. Yu, and S. K. Behera, 2017: A possible explanation for the divergent projection of ENSO amplitude change under global warming. *Climate Dyn.*, **49**, 3799−3811, doi: 10.1007/s00382-017-3544-x.

Chen, M., and T. Li, 2017: Why 1986 El Niño and 2005 La Niña evolved different from a typical El Niño and La Niña. *Climate Dyn.*, doi:10.1007/s00382-017-3852-1.

Chung, P.-H., and T. Li, 2013: Interdecadal relationship between the mean State and El Niño types. *J. Climate*, **26**, 361−379.

Dee, D. P., and co-authors, 2011: The ERA-Interim reanalysis: Configuration and performance of the data assimilation system. *Quart. J. Roy. Meteor. Soc.*, **137**, 553−597.

Fang, X.-H., F. Zheng, and J. Zhu, 2015: The cloud-radiative effect when simulating strength asymmetry in two types of El Niño events using CMIP5 models. *J. Geophys. Res. Oceans*, **120**, 4357−4369.

Feng, J., J. Li, F. Zheng, F. Xie, and C. Sun, 2016a: Contrasting impacts of developing phases of two types of El Niño on southern China rainfall. *J. Meteor. Soc. Japan. Ser. II*, **94**, 359−370.

Feng, J., J. Li, J. Zhu, and H. Liao, 2016b: Influences of El Niño Modoki event 1994/1995 on aerosol concentrations over southern China. *J. Geophys. Res. Atmos.*, **121**, doi:10.1002/2015JD023659.

Feng, J., W. Chen, and Y. Li, 2017: Asymmetry of the winter extra-tropical teleconnections associated with two types of ENSO. *Climate Dyn.*, **48**, 2135−2151.

Hartmann, D. L., and D. A. Short, 1980: On the use of earth radiation budget statistics for studies of clouds and climate. *J. Atmos. Sci.*, **37**, 1233−1250.

Houghton, J. T., Y. Ding, D. J. Griggs, M. Noguer, P. J. van der Linden, X. Dai, K. Maskel, and C. A. Johnson, Eds., 2001: *Climate Change 2001: The Scientific Basis*. Cambridge University Press, 881 pp.

Hu, X., S. Yang, and M. Cai, 2016: Contrasting the eastern Pacific El Niño and the central Pacific El Niño: process-based feedback attribution. *Climate Dyn.*, **47**, 2413−2424.

Hu, X., M. Cai, S. Yang, and Z. Wu, 2017: Delineation of thermodynamic and dynamic responses to sea surface temperature forcing associated with El Niño. *Climate Dyn.*, doi:10.1007/s00382-017-3711-0.

Huffman, G. J., R. F. Adler, D. T. Bolvin, and G. Gu, 2009: Improving the global precipitation record: GPCP Version 2.1. *Geophys. Res. Lett.*, **36**, L17808.

Kao, H. Y., and J. Y. Yu, 2009: Contrasting eastern-Pacific and central-Pacific types of ENSO. *J. Climate*, **22**, 615−632.

Kiehl, J. T., and K. E. Trenberth, 1997: Earth's annual global mean energy budget. *Bull. Amer. Meteor. Soc.*, **78**, 197−208.

Kug, J. S., F. F. Jin, and S. I. An, 2009: Two types of El Niño events: cold tongue El Niño and warm pool El Niño. *J. Climate*, **22**, 1499−1515.

Li, L., 2015: The role of moist processes in shortwave radiative feedback during ENSO in the CMIP5 models. *J. Climate*, **28**, 9892−9908.

Li, L., B. Wang, and G. J. Zhang, 2014: The role of nonconvective condensation processes in response of surface shortwave cloud radiative forcing to El Niño warming. *J. Climate*, **27**, 6721−6736.

Philander, S. G. H., 1990: *El Niño, La Niña, and the Southern Oscillation*. International Geophysics Series, Vol. 46, Academic Press, 293 pp.

Ramanathan, V., R. D. Cess, E. F. Harrison, P. Minnis, B. R. Barkstrom, E. Ahmad, and D. Hartmann, 1989: Cloud-radiative forcing and climate: Results from the earth radiation budget experiment. *Science*, **243**, 57−63.

Rayner, N. A., and co-authors, 2003: Global analyses of sea surface temperature, sea ice, and night marine air temperature since the late nineteenth century. *J. Geophys. Res. Atmos.*, **108**, 4407.

Ren, H.-L., and F.-F. Jin, 2011: Niño indices for two types of ENSO. *Geophys. Res. Lett.*, **38**, L04704.

Schneider, E. K., B. P. Kirtman, and R. S. Lindzen, 1999: Tropospheric water vapor and climate sensitivity. *J. Atmos. Sci.*, **56**, 1649−1658.

Soden, B. J., 1997: Variations in the tropical greenhouse effect during El Niño. *J. Climate*, **10**, 1050−1055.

Soden, B. J., and I. M. Held, 2006: An assessment of climate feedbacks in coupled ocean–atmosphere models. *J. Climate*, **19**, 3354−3360.

Stephens, G. L., 2005: Cloud feedbacks in the climate system: A critical review. *J. Climate*, **18**, 237−273.

Su, J., R. Zhang, and T. Li, 2014: The initiation and developing mechanisms of central Pacific El Niños. *J. Climate*, **27**, 4473−4485.

Sun, D. Z., and I. M. Held, 1996: A comparison of modeled and observed relationships between interannual variations of water vapor and temperature. *J. Climate*, **9**, 665−675.

Sun, D. Z., J. Fasullo, T. Zhang, and A. Roubicek, 2003: On the radiative and dynamical feedbacks over the equatorial Pacific cold tongue. *J. Climate*, **16**, 2425−2432.

Sun, D. Z., and co-authors, 2006: Radiative and dynamical feedbacks over the equatorial cold tongue: results from nine atmospheric GCMs. *J. Climate*, **19**, 4059-4074.

Sun, D. Z., Y. Yu, and T. Zhang, 2009: Tropical water vapor and cloud feedbacks in climate models: A further assessment using coupled simulations. *J. Climate*, **22**, 1287−1304.

Wang, L., and L. Chen, 2016: Interannual variation of convectively-coupled equatorial waves and their association with environmental factors. *Dyn. Atmos. Oceans*, **76**, 116−126, doi:10.1016/j.dynatmoce.2016.10.004.

Wang, L., and L. Chen, 2017a: Effect of basic state on seasonal variation of convectively coupled Rossby wave. *Dyn. Atmos. Oceans*, **77**, 54−63, doi:10.1016/j.dynatmoce.2016.11.002.

Wang, L., and L. Chen, 2017b: Interannual variation of the Asian-Pacific oscillation. *Dyn. Atmos. Oceans*, **77**, 17−25, doi:10.1016/j.dynatmoce.2016.10.009.

Weng, H., K. Ashok, S. K. Behera, S. A. Rao, and T. Yamagata, 2007: Impacts of recent El Niño Modoki on dry/wet conditions in the Pacific rim during boreal summer. *Climate Dyn.*, **29**, 113−129.

Wu, C., T. Zhou, D.-Z. Sun, and Q. Bao, 2011: Water vapor and cloud radiative forcings over the Pacific Ocean simulated by the LASG/IAP AGCM: Sensitivity to convection schemes. *Adv. Atoms. Sci.*, **28**, 80−98.

Xiang, B., B. Wang, and T. Li, 2013: A new paradigm for the predominance of standing Central Pacific Warming after the late 1990s. *Climate Dyn.*, **41**, 327−340.

Xiang, B., B. Wang, Q. Ding, F. F. Jin, X. Fu, and H.-J. Kim, 2012: Reduction of the thermocline feedback associated with mean SST bias in ENSO simulation. *Climate Dyn.*, **39**, 1413−1430.

Xu, K., R. X. Huang, W. Wang, C. Zhu, and R. Lu, 2017a: Thermocline fluctuations in the equatorial Pacific related to the two types of El Niño events. *J. Climate*, **30**, 6611−6627.

Xu, K., C.-Y. Tam, C. Zhu, B. Liu, and W. Wang, 2017b: CMIP5 projections of two types of El Niño and their related tropical precipitation in the twenty-first century. *J. Climate*, **30**, 849−864.

Xu, K., Q.-L. Huang, C.-Y. Tam, W. Wang, S. Chen, and C. Zhu, 2018: Roles of tropical SST patterns during two types of ENSO in modulating wintertime rainfall over southern China. *Climate Dyn.*

Yang, S., Z. Li, J.-Y. Yu, X. Hu, W. Dong, and S. He, 2018: El Niño–Southern oscillation and its impact in the changing climate. *Nat. Sci. Rev.*, nwy046-nwy046, doi:10.1093/nsr/nwy046.

Zhang, T., and D. Z. Sun, 2008: What causes the excessive response of clear-sky greenhouse effect to El Niño warming in community atmosphere models? *J. Geophys. Res.*, **113**, D02108.

Zhang, Y., W. B. Rossow, A. A. Lacis, V. Oinas, and M. I. Mishchenko, 2004: Calculation of radiative fluxes from the surface to top of atmosphere based on ISCCP and other global data sets: Refinements of the radiative transfer model and the input data. *J. Geophys. Res. Atmos.*, **109**, D19105.

Zheng, F., X.-H. Fang, J.-Y. Yu, and J. Zhu, 2014: Asymmetry of the Bjerknes positive feedback between the two types of El Niño. *Geophys. Res. Lett.*, **41**, doi:10.1002/2014GL062125.

Zhu, P., J. J. Hack, J. T. Kiehl, and C. S. Bretherton, 2007: Climate sensitivity of tropical and subtropical marine low cloud amount to ENSO and global warming due to doubled CO2. *J. Geophys. Res. Atmos.*, **112**, D17108.

Zhou, T., B. Wu, and L. Dong, 2014: Advances in research of ENSO changes and the associated impacts on Asian-Pacific climate. *Asia-Pac. J. Atmos. Sci.*, **50**, 405−422.